

Atomic arrangement of van der Waals heterostructures using X-ray scattering and crystal truncation rod analysis

Ryung Kim^{a†}, Byoung Ki Choi^{b,c†}, Kyeong Jun Lee^a, Hyuk Jin Kim^b, Hyun Hwi Lee^d, Tae Gyu Rhee^{b,e}, Yeong Gwang Khim^{b,e}, Young Jun Chang^{b,e}, and Seo Hyoung Chang^{a*}

^a*Department of Physics, Chung-Ang University, Seoul 60974, Republic of Korea*

^b*Department of Physics, University of Seoul, Seoul 02504, Republic of Korea*

^c*Advanced Light Source (ALS), E. O. Lawrence Berkeley National Laboratory, Berkeley, California 94720, USA*

^d*Pohang Accelerator Laboratory (PAL), Pohang University of Science and Technology (POSTECH), Pohang 37673, Republic of Korea*

^e*Department of Smart Cities, University of Seoul, Seoul 02504, Republic of Korea*

Vanadium diselenide (VSe₂) has intriguing physical properties such as unexpected ferromagnetism at the two-dimensional limit. However, the experimental results for room temperature ferromagnetism are still controversial and depend on the detailed crystal structure and stoichiometry. Here we introduce crystal truncation rod (CTR) analysis to investigate the atomic arrangement of bilayer VSe₂ and bilayer graphene (BLG) heterostructures grown on a 6H-SiC(0001) substrate. Using non-destructive CTR analysis, we were able to obtain electron density profiles and detailed crystal structure of the VSe₂/BLG heterostructures. Specifically, the out-of-plane lattice parameters of each VSe₂ layer were modulated by the interface compared to that of the bulk VSe₂ 1T phase. The atomic arrangement of the VSe₂/BLG heterostructure provides deeper understanding and insight for elucidating the magnetic properties of the van der Waals heterostructure.

e-mail: cshyoung@cau.ac.kr

Keywords: Transition-metal dichalcogenide, van der Waals, Vanadium diselenide, X ray scattering, Crystal truncation rod analysis

1. Introduction

Transition metal dichalcogenides (TMDCs) have been intensively investigated due to their intriguing physical properties at the two-dimensional (2D) limit [1–3]. Because of their weak van der Waals (vdW) interactions compared to covalent bonds, TMDCs and graphene are known as ideal platforms for investigating intriguing 2D physics and fabricating heterostructures, even when controlling twisted angles [4,5]. For instance, Mott insulating state and superconductivity of twisted bilayer graphene emerged from strongly correlated electrons [6]. Moreover, the charge-density wave (CDW) and magnetic properties of the heterostructures can be modulated by interlayer coupling, reduced dimensionality, and thermal fluctuations [7]. Understanding the interfacial structure of TMDC-based heterostructures is important for exploring novel phenomena and engineering their functionalities.

Compared to the paramagnetic state of the Vanadium diselenide (VSe_2), unexpected ferromagnetism at room temperature of monolayer 1T VSe_2 has been experimentally observed and extensively investigated. However, scanning tunneling microscopy (STM) and angle-resolved photoemission spectroscopy (ARPES) have measured CDW phases with $4 \times 4 \times 3$ periodicity of bulk and distinct periodicity of 2D, which can normally prohibit the appearance of ferromagnetic orders [8,9]. In addition, there have been inconsistencies in numerous experiments on the magnetic moments, which are believed to be due to the quality of samples, e.g., different cation / anion stoichiometries, strain, and crystal structures, and have been controversial to date [10,11].

The interfacial effects of VSe_2 heterostructures can modify electronic structures and are closely related to exotic physical properties such as enhanced magnetic moments and flat bands [11,12]. However, the understanding of the interfacial structure of VSe_2 heterostructures is still not satisfactory due to experimental technical difficulties. Therefore, resolving atomic-level interfacial structures in VSe_2 -based heterostructures is very critical for unveiling and determining their intrinsic physical properties.

Here, we investigate the atomic arrangement of bilayer VSe₂/bilayer graphene (BLG) heterostructure using surface X-ray scattering and crystal truncation rod (CTR) analysis. To determine the out-of-plane and in-plane lattice parameters of the bilayer VSe₂/BLG heterostructure, a model system was constructed through simulation and fitting analysis based on the Fourier transformation of complex structure factors. We then obtained appropriate electron density profiles of bilayer VSe₂, BLG, and reconstructed SiC substrates from the samples, which is consistent with the previous study [13]. Resonant energy dependence and off-specular CTR analysis were used to confirm detailed in-plane lattice information of the bilayer VSe₂/BLG heterostructure.

2. Experiment

The high-quality epitaxial thin films were grown on 6H-SiC (001) substrates (Crystal Bank at Pusan National University) and fabricated using a home-built molecular beam epitaxy (MBE) deposition. The substrate was annealed to form BLG on the Si. VSe₂ ultrathin films were grown on BLG with a base pressure of 2×10^{-10} Torr. V (99.8%) and Se (99.999%) were simultaneously evaporated by an electron beam evaporator (EFM3, Omicron GmbH) and a Knudsen cell (Effucell Co.). A deposition temperature of 250°C was used and film growth was monitored by reflection-high energy electron diffraction (RHEED). The growth rate was 20 min per monolayer and the samples were post-annealed at 350°C for 30 min. Detailed growth conditions were described elsewhere [14].

X-ray diffraction (XRD) measurements were performed using a laboratory X-ray source with Cu K_α radiation and a high-resolution X-ray diffractometer (Bruker AXS D8). For high resolution, Göbel mirror and Ge(004) two bounce monochromatic setup were used on the incident beam side. X-ray scattering studies were performed using a synchrotron radiation source at beamline 5A of Pohang Light Source II (PLS II, South Korea). The typical size of the focused beam was about 700×50 μm². A six-circle Huber goniometer with a 2D detector (PILATUS II 200K, Dectris) was used for the higher reciprocal lattice spaces and resolution. The X-ray energies for specular and off-specular rod scans were 11.85 keV and 12.55 keV, respectively, as shown in Fig. 2 and Fig. 4, respectively. A Matlab program and a python-based program (e.g., jupyter notebook) were used for 2D detector data

analysis and the fitting calculations, respectively. Detailed fitting calculation was described in the Section 1 in the Supplementary Information.

3. Results and discussion.

Figure 1(a) shows a schematic of a 1T VSe₂/BLG heterostructure. VSe₂ mainly exhibits two polymorphs: 1T phase and 2H phase. The 1T structure refers to an octahedral in which transition metal (V) is sandwiched between the chalcogen layer (Se) and the reversed chalcogen layer, and the 2H phase has two symmetrical equilateral triangles of chalcogen layers. Although theoretical studies proposed two polymorphs for room temperature ferromagnetism, the 1T VSe₂ phase has been reported in most experiments [15–17]. Using X-ray diffraction and TEM measurements, single crystals and thin films of several nanometers are known to be 1T VSe₂ phases. In particular, our monolayer and bilayer VSe₂ samples fabricated with MBE were identified as 1T VSe₂ phases using STM [14].

Atomic-level crystal structure verification of VSe₂ heterostructure samples is a prerequisite for understanding physical properties such as unsolved ferromagnetic orders, but it is still difficult using non-destructive experimental methods. Bulk crystal of 1T VSe₂ is shown in Fig. 1(b) with the lattice parameter with $a=b=3.3 \text{ \AA}$, $c=6.1 \text{ \AA}$, $\gamma=120^\circ$ (space group $\bar{P}3m1$) [17,18]. Using the TEM, the out-of-plane lattice parameter of VSe₂ nanosheets can be varied up to 5.88 \AA , which was significantly different from that of the bulk samples. STM was only able to confirm in-plane lattice parameters, $3.2\text{--}3.4 \text{ \AA}$ [14,19]. To identify the lattice parameters of the bilayer VSe₂ heterostructure sample, we attempted to perform XRD measurements using a laboratory X-ray source as shown in Fig. 1(c). Our VSe₂ heterostructure sample consists of a bilayer VSe₂ (approximately 1.2 nm), bilayer graphene ($\sim 0.6 \text{ nm}$), and a 500 \mu m thick SiC substrate. Figure 1(c) demonstrates that the scattering pattern of bilayer VSe₂ heterostructure samples was exactly same as that of the SiC substrate because of the weak scattering cross-section in the XRD measurement.

We investigated the buried interfacial structures of the VSe₂ heterostructure as shown in Fig. 2 by performing synchrotron-based X-ray scattering with a beam energy of 11.85 keV. Conventional

XRD usually measures the average value of the lattice parameters of a thin film. Here, we introduce CTR scattering, a powerful tool for resolving the interfacial structure and lattice parameters of individual layers at the sub-Å scale [20–22]. CTR is a diffraction patterns derived from the crystalline surface of a high-quality sample, indicating that there is a scattering intensity between typical Bragg peaks detectable by conventional XRD due to the Fourier transformation with truncations or broken periodicity [23]. To clearly detect these weak signals in the collected intensities, background subtraction and careful geometrical correction were required. Then, by fitting the CTR scattering with or without a model, detailed interfacial structures can be determined with atomic-level resolution. Note that CTR scattering can also use off-specular rod scans for resolving in-plane lattice information. Here, we performed a specular rod scan along the (00L) direction in the reciprocal lattice space to confirm the surface and interfacial structures of VSe₂ heterostructures.

To describe the interfacial structure with atomic-level resolution, we measured the CTR scattering of monolayer and bilayer VSe₂ samples, as shown in Fig. 2(a). Our monolayer and bilayer samples have some domains with different thicknesses, but they are named as major domains of nominal thickness [see Fig. S1 and Fig. S2 in the Supplementary Information]. The CTR data of the monolayer VSe₂ heterostructure was distinguishable by comparison with the reported CTR result of the bilayer graphene on SiC [13]. The main features due to the monolayer VSe₂ heterostructure were dip features at around $L = 7.733$ and subsequential peaks, indicated by (c) in Fig. 2(a). Evidently, the diffraction pattern of the substrate (half-infinite periodic layers) produces features similar to delta functions, especially in the vicinity of SiC(0006) and SiC(00012).

To explore the thickness dependence of VSe₂, we compared the CTR data of bilayer VSe₂ samples, indicating that the intensity of VSe₂(002) is clearly stronger than that of monolayer VSe₂ samples. Conventional XRD analysis obtained from VSe₂(002) reflection in bilayer VSe₂ provided that the out-of-plane lattice parameter was approximately 6.13 ± 0.1 Å. However, the value was not layer-resolved but the average of lattice parameters obtained from monolayer and bilayer VSe₂. In particular, the CTR data represents broad peaks with relatively weak intensities originated from the interference between VSe₂, graphene, and the surface modulation of SiC substrate. Therefore, to

obtain an atomic-level accurate interfacial structure, CTR analysis using a fine-fitting model is required. Then, we can resolve the lattice parameters of each VSe₂ layer.

For the scattering vector along the 00L direction, the diffracted CTR signal and Bragg peak can be detected using a pixel 2D area detector. Since CTR intensity occur when the surface is truncated, the CTR signal is highly dependent on the dimensionality and modulation of surface structure. As shown in Fig. 2(b), area detector near the Bragg reflection, denoted by (b) in Fig. 2(a), can identify the CTR intensity with typical Gaussian shape (red box) and Bragg-related peak (white box) along the 00L direction in the reciprocal lattice space [24]. The CTR signal was maintained up to (0014) and showed the anti-Bragg reflection, denoted by (c) in Fig. 2(a) and Fig. 2(c), respectively. This indicates that the VSe₂ heterostructure was a high-quality sample with a well-defined SiC surface and the following interface. Figure 2(d) shows stronger CTR intensity compared to monolayer VSe₂, indicating a clear thickness dependence of the CTR signal of the VSe₂ heterostructure.

To gain further insight into the detailed atomic arrangement of bilayer VSe₂/BLG heterostructure, simulation and CTR fitting were performed based on the scattering factor, F_{total} , as shown in Fig. 3(a). The CTR intensity is proportional to F_{total} and can be calculated as following

$$F_{total} = \sum_j \theta_j (f_j + f' + i \cdot f'') e^{-iqr_j} e^{-\frac{\sigma_j^2 q^2}{2}} e^{-B_j q^2} \cdot C_R \quad (1)$$

where j is the index of each atom, q is the momentum transfer, f_j is atomic form factor, f' , f'' is the energy dependent atomic form factor, and B_j is the Debye Waller factor. Note that σ_j is the standard deviation of each atomic layer distribution of and C_R is the roughness factor [25–31] of the sample. Instead of controlling the roughness factor, the contribution of islands and domains with three buffer layers related to the graphene has been considered [See Section on the CTR analysis and Fig. S1 in the Supplementary Information].

Figure 3(b) shows the quantitative analysis results by fitting the model system. For the fitting analysis, we adjusted the occupancy and displacement of bulk Si and C atoms in the top-level SiC unit

cell, Si_{Bulk} and C_{Bulk} , respectively, compatible with the reference values [13]. The buffer layer was formed between the SiC substrate and graphene and is separated from each other [32,33]. The buffer layer was reconstructed and composed of two carbon atoms S1 and S2 located at $2.31 \pm 0.3 \text{ \AA}$ and $1.91 \pm 0.3 \text{ \AA}$, respectively. The occupancy values of S1 and S2 were 1 and 0.89, respectively. The model had bilayer graphene in which the first graphene G1 and the second graphene G2 were positioned at 5.51 and 8.71 \AA , respectively, as shown in Fig. 3(c). Our model had three domains consisting of buffer-only, monolayer graphene, and bilayer graphene with coverages of 0.23, 0.47, and 0.3, respectively. The G1 and G2 layers showed reasonable positions and distributions of 0.23 and 0.22 \AA , respectively. The electron density profiles obtained from the fitting reveals the detailed occupancy and displacement of each element [see Fig. S1 in the Supplementary Information].

Figure 3(c) represents the out-of-plane lattice parameters of the bilayer VSe_2 , graphene layer, and SiC substrate. Specifically, the center positions of the first and second VSe_2 layers were located at 4.625 \AA and 10.640 \AA from the last graphene layer, respectively. In the bilayer VSe_2 model, there are multiple VSe_2 domains with different thicknesses of VSe_2 , mainly bilayer VSe_2 with coverage of 0.67 each. In the first VSe_2 layer, the occupancy of top and bottom Se layers labeled as Se(I) and Se(II), were 1 and 0.92, respectively. In addition, the occupancy of Se(I) and Se(II) in the second VSe_2 layer were 0.87 and 1, respectively. Surprisingly, we found that the top and bottom Se layer spacing of the first VSe_2 layer between layers was 2.87 \AA . This is because the spacing between the two Se layers in the bulk sample is usually 3.10 \AA , which is similar with the spacing between the top and bottom Se layers of the second VSe_2 layer. Compared with previously reported lattice parameters of 1T VSe_2 , the out-of-plane lattice parameter of the first VSe_2 layer of the heterostructure was compressed to about 6.06 \AA , while the lattice parameter of the second layer was nearly stretched by almost 6.13 \AA . The average value of two layers was nearly identical with that of bulk 1T VSe_2 . Theoretical and experimental studies have proposed that the distance between V and Se atom can lead to the emergence of ferromagnetic orders originated from the modification of electronic structure, orbital states, Se stoichiometry, and structure phase transitions.

To elucidate the in-plane alignment and bond length of the bilayer VSe₂ heterostructure, we performed phi-scan and off-specular CTR measurements, as shown in Fig. 4. However, the precise experimental observation of the in-plane alignment of vdW-based heterostructure is an important unresolved research topic. This is because the weak vdW interaction between two layers can lead to quasi-stable structures that differ significantly from the covalent bond-based heterostructures. Figure 4(a) shows a schematic diagram of the possible in-plane alignment of the VSe₂ layer and the SiC substrate in reciprocal space, showing approximately 30° rotation in the in-plane direction of VSe₂[100] relative to the SiC[1010] substrate. As shown in Fig. 4(b), we found that the peak spacing of the measured phi-scan at (0.518 0.518 2.4) reflection was about 60° in sixfold symmetry. Note that the average value of the full width half maximum (FWHM) values of reflections in the phi scan was 6.6°, which was in good agreement with the reported value (approximately 5°) measured by LEED [14].

A possible origin of the six-fold peaks from the heterostructure is the presence of domains in the graphene, 2H VSe₂ or 1T VSe₂ phase, with different in-plane orientations. To rule out the possibility of a graphene layer, we measured anomalous x-ray diffraction using Se K-edge. We clearly found absorption features near the Se K-edge, indicating the (0.518 0.518 2.4) reflection originated from the VSe₂ layer. As shown in Fig. 4(d), the calculated in-plane lattice parameter was 3.44Å, which was about 4.2% larger than that of bulk 1T VSe₂ phase. In-plane CTR simulations (red line in Fig. 4(d)) of bilayer VSe₂/bilayer graphene heterostructure grown on SiC substrate reproduce the experimental results obtained from the (0.518 0.518 2.4) reflection (black dots in Fig. 4(d)). The model included various in-plane orientations of 1T VSe₂ phase rather than the domains of 2H phase. Although the in-plane CTR measurements and analyses on the vdW heterostructures were so challengeable due to inherent weak and broad signals associated with the low dimension, CTR have provided new opportunities to identify atomic-level interfacial structures and to explore the intrinsic physical properties of vdW heterostructures.

4. Conclusions

In summary, we resolved the atomic-level structural properties of the bilayer VSe₂/bilayer graphene (BLG) heterostructures using crystal truncation rod (CTR) analysis. CTR analysis was able to address one-dimensional atomic arrangement of the VSe₂/BLG heterostructures. We confirmed the bilayer VSe₂ layer was a 1T phase with different in-plane domains. Furthermore, we quantitatively defined the electron density profiles leading to the atomic-level positions of elements and out-of-plane and in-plane lattice parameters of each layer of the heterostructure. CTR analysis provides a novel experimental method to directly measure detailed structural properties of van der Waals heterostructure systems and explore their intriguing functionalities.

Acknowledgments

The work was supported by the Chung-Ang University Graduate Research Scholarship in 2021 (awarded to R.K.) and was supported by Basic Science Research Programs through the National Research Foundation of Korea (Grants No. No. 2020R1C1C1012424). This work was supported by MOLIT as [Innovative Talent Education Program for Smart City].

Figure Captions

Figure 1 | VSe₂ heterostructures. (a) Schematic of bilayer VSe₂/bilayer graphene (BLG) grown on 6H-SiC substrate. (b) Top and side view of 1T VSe₂ bulk structure and its lattice parameters. (c) X-ray diffraction (XRD) using a laboratory source of bilayer VSe₂/BLG heterostructure samples grown on 6H-SiC substrate (red line) and 6H-SiC substrate (black line). The index was assigned to the reciprocal lattice units (r. l. u.) of the 6H-SiC substrate.

Figure 2 | Crystal truncation rod (CTR) scattering of VSe₂/BLG heterostructure. (a) CTR measurements of monolayer (blue) and bilayer (red) VSe₂ heterostructures measured along the out-of-plane direction, 00L. The (0 0 L) reflection of VSe₂ and the image of two-dimension (2D) area detector were indicated by inverted triangles and arrows, respectively. (b) 2D image of a monolayer VSe₂/BLG heterostructure sample measured at L=5.87 represents the CTR (red box) and Bragg peak of the substrate (white box). (c) 2D image measured at L=7.73 shows a representative anti-Bragg peak of our sample. (d) 2D image of monolayer VSe₂/BLG heterostructure sample measured at L=9.4.

Figure 3 | CTR analysis of bilayer VSe₂/BLG heterostructure based on the model system. (a) CTR measurement data (black circle) and fitting result based on our model (red line). Green dashed line is a representative simulation based on lattice parameters of bulk 1T VSe₂. (b) Detailed estimated layer spacing of each atomic layer. (c) Out-of-plane lattice parameters of Buff., G1, G2, and VSe₂, which were the C buffer layer on the SiC substrate, first graphene, second graphene, VSe₂ layers, respectively. The blue and brown lines correspond to the Si and C layers, respectively. Error bars are the average distributions of domains.

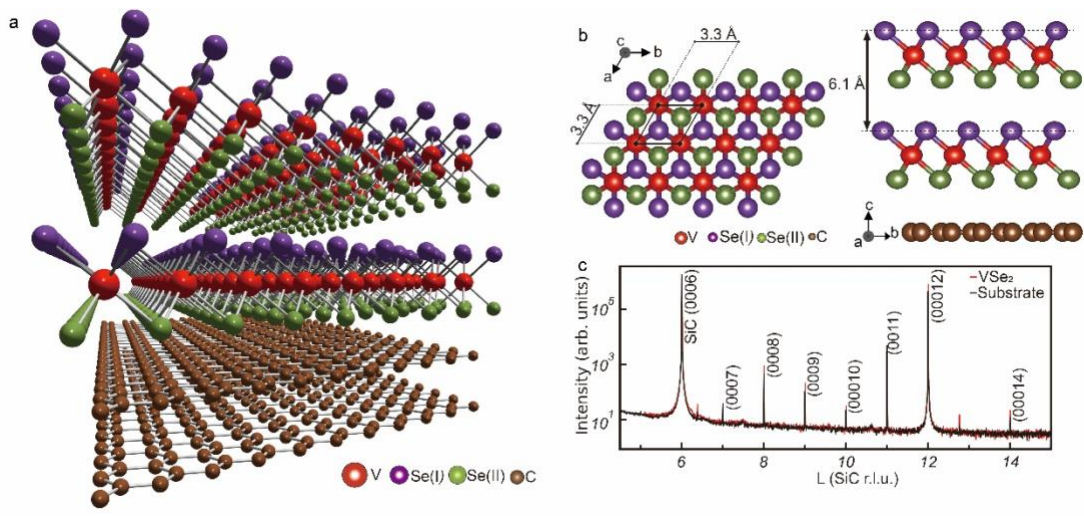
Figure 4 | Off-specular CTR measurements of bilayer VSe₂/BLG heterostructures for in-plane lattice

parameters. (a) A schematic of the reciprocal lattice vectors, a^* and b^* , of SiC and VSe₂ layers. (b) Phi scan measurement taken at (0.518, 0.518, 2.4). (c) Resonant energy scan measured at (0.518, 0.518, 2.4) near Se K edge. (d) Off-specular CTR measurement along (0.518 0.518 L) and a simulation result based on the model of bilayer VSe₂/BLG heterostructures, denoted by black dot and red line, respectively. Gray dashed line is the noise level.

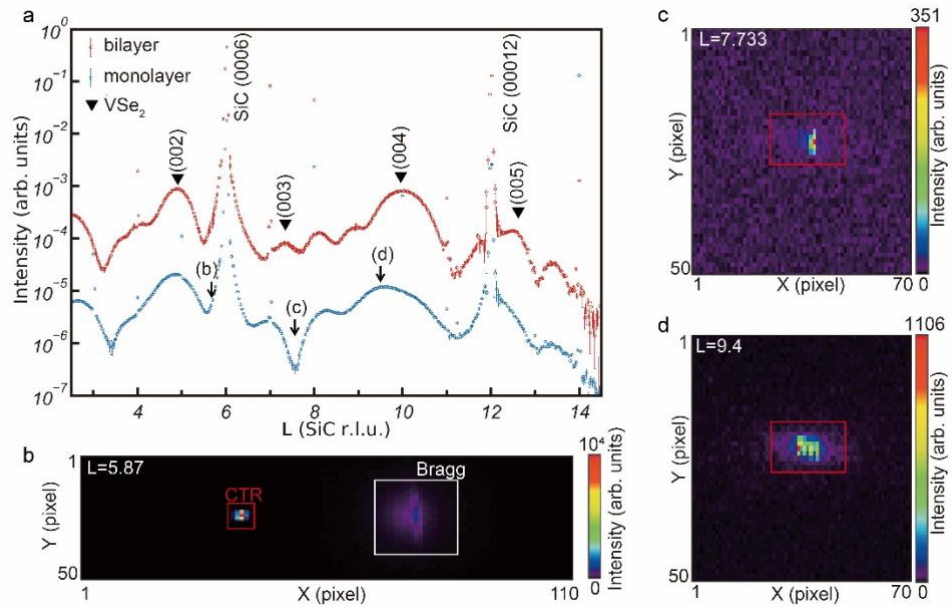
Reference

- [1] M. Calandra, I.I. Mazin, F. Mauri, Effect of dimensionality on the charge-density wave in few-layer 2 H - NbSe₂, *Phys. Rev. B.* 80 (2009) 241108. <https://doi.org/10.1103/PhysRevB.80.241108>.
- [2] H. Li, Q. Zhang, C.C.R. Yap, B.K. Tay, T.H.T. Edwin, A. Olivier, D. Baillargeat, From Bulk to Monolayer MoS₂: Evolution of Raman Scattering, *Adv. Funct. Mater.* 22 (2012) 1385–1390. <https://doi.org/10.1002/adfm.201102111>.
- [3] P. Darancet, A.J. Millis, C.A. Marianetti, Three-dimensional metallic and two-dimensional insulating behavior in octahedral tantalum dichalcogenides, *Phys. Rev. B.* 90 (2014) 045134. <https://doi.org/10.1103/PhysRevB.90.045134>.
- [4] W. Chen, Z. Sun, Z. Wang, L. Gu, X. Xu, S. Wu, C. Gao, Direct observation of van der Waals stacking-dependent interlayer magnetism, *Science.* 366 (2019) 983–987. <https://doi.org/10.1126/science.aav1937>.
- [5] L. Zhang, Z. Zhang, F. Wu, D. Wang, R. Gogna, S. Hou, K. Watanabe, T. Taniguchi, K. Kulkarni, T. Kuo, S.R. Forrest, H. Deng, Twist-angle dependence of moiré excitons in WS₂/MoSe₂ heterobilayers, *Nat. Commun.* 11 (2020) 5888. <https://doi.org/10.1038/s41467-020-19466-6>.
- [6] Y. Cao, V. Fatemi, S. Fang, K. Watanabe, T. Taniguchi, E. Kaxiras, P. Jarillo-Herrero, Unconventional superconductivity in magic-angle graphene superlattices, *Nature.* 556 (2018) 43–50. <https://doi.org/10.1038/nature26160>.
- [7] D. Lin, S. Li, J. Wen, H. Berger, L. Forró, H. Zhou, S. Jia, T. Taniguchi, K. Watanabe, X. Xi, M.S. Bahramy, Patterns and driving forces of dimensionality-dependent charge density waves in 2H-type transition metal dichalcogenides, *Nat. Commun.* 11 (2020) 2406. <https://doi.org/10.1038/s41467-020-15715-w>.
- [8] G. Duvjir, B.K. Choi, T.T. Ly, N.H. Lam, S.-H. Chun, K. Jang, A. Soon, Y.J. Chang, J. Kim, Novel polymorphic phase of two-dimensional VSe₂: the 1T' structure and its lattice dynamics, *Nanoscale.* 11 (2019) 20096–20101. <https://doi.org/10.1039/C9NR06076F>.
- [9] G. Duvjir, B.K. Choi, T. Thi Ly, N.H. Lam, K. Jang, D.D. Dung, Y.J. Chang, J. Kim, Multiple charge density wave phases of monolayer VSe₂ manifested by graphene substrates, *Nanotechnology.* 32 (2021) 364002. <https://doi.org/10.1088/1361-6528/ac06f3>.
- [10] W. Yu, J. Li, T.S. Herng, Z. Wang, X. Zhao, X. Chi, W. Fu, I. Abdelwahab, J. Zhou, J. Dan, Z. Chen, Z. Chen, Z. Li, J. Lu, S.J. Pennycook, Y.P. Feng, J. Ding, K.P. Loh, Chemically Exfoliated VSe₂ Monolayers with Room-Temperature Ferromagnetism, *Adv. Mater.* 31 (2019) 1903779. <https://doi.org/10.1002/adma.201903779>.
- [11] M. Bonilla, S. Kolekar, Y. Ma, H.C. Diaz, V. Kalappattil, R. Das, T. Eggers, H.R. Gutierrez, M.-H. Phan, M. Batzill, Strong room-temperature ferromagnetism in VSe₂ monolayers on van der Waals substrates, *Nat. Nanotechnol.* 13 (2018) 289–293. <https://doi.org/10.1038/s41565-018-0063-9>.
- [12] T. Yilmaz, X. Tong, Z. Dai, J.T. Sadowski, E.F. Schwier, K. Shimada, S. Hwang, K. Kisslinger, K. Kaznatcheev, E. Vescovo, B. Sinkovic, Emergent flat band electronic structure in a VSe₂/Bi₂Se₃ heterostructure, *Commun. Mater.* 2 (2021) 11. <https://doi.org/10.1038/s43246-020-00115-w>.
- [13] J.D. Emery, B. Dettlefs, H.J. Karmel, L.O. Nyakiti, D.K. Gaskill, M.C. Hersam, J. Zegenhagen, M.J. Bedzyk, Chemically Resolved Interface Structure of Epitaxial Graphene on SiC(0001), *Phys. Rev. Lett.* (2013) 5.
- [14] G. Duvjir, B.K. Choi, I. Jang, S. Ulstrup, S. Kang, T. Thi Ly, S. Kim, Y.H. Choi, C. Jozwiak, A. Bostwick, E. Rotenberg, J.-G. Park, R. Sankar, K.-S. Kim, J. Kim, Y.J. Chang, Emergence of a Metal–Insulator Transition and High-Temperature Charge-Density Waves in VSe₂ at the Monolayer Limit, *Nano Lett.* 18 (2018) 5432–5438. <https://doi.org/10.1021/acs.nanolett.8b01764>.
- [15] E. Spiecker, A.K. Schmid, A.M. Minor, U. Dahmen, S. Hollensteiner, W. Jäger, Self-Assembled Nanofold Network Formation on Layered Crystal Surfaces during Metal Intercalation, *Phys. Rev. Lett.* 96 (2006) 086401. <https://doi.org/10.1103/PhysRevLett.96.086401>.
- [16] R. Atkins, M. Dolgos, A. Fiedler, C. Grosse, S.F. Fischer, S.P. Rudin, D.C. Johnson, Synthesis and Systematic Trends in Structure and Electrical Properties of [(SnSe)_{1.15}]_m (VSe₂)₁, *m* = 1, 2, 3, and 4, *Chem. Mater.* 26 (2014) 2862–2872. <https://doi.org/10.1021/cm5004774>.
- [17] M. Bayard, M.J. Sienko, Anomalous electrical and magnetic properties of vanadium diselenide, *J. Solid State Chem.* 19 (1976) 325–329. [https://doi.org/10.1016/0022-4596\(76\)90184-5](https://doi.org/10.1016/0022-4596(76)90184-5).
- [18] A. Feroze, H.R. Na, Y.C. Park, J.-H. Jun, M.-H. Jung, J.-H. Lee, J.-H. Kim, M.-J. Seong, S. Hong, S.-H. Chun, S. Lee, In-Depth Structural Characterization of 1T-VSe₂ Single Crystals Grown by Chemical Vapor Transport, *Cryst. Growth Des.* 20 (2020) 2860–2865. <https://doi.org/10.1021/acs.cgd.0c00219>.
- [19] G. Chen, S.T. Howard, A.B. Maghirang, K. Nguyen Cong, R.A.B. Villaos, L.-Y. Feng, K. Cai, S.C. Ganguli, W. Swiech, E. Morosan, I.I. Oleynik, F.-C. Chuang, H. Lin, V. Madhavan, Correlating structural, electronic, and magnetic properties of epitaxial V Se₂ thin films, *Phys. Rev. B.* 102 (2020) 115149.

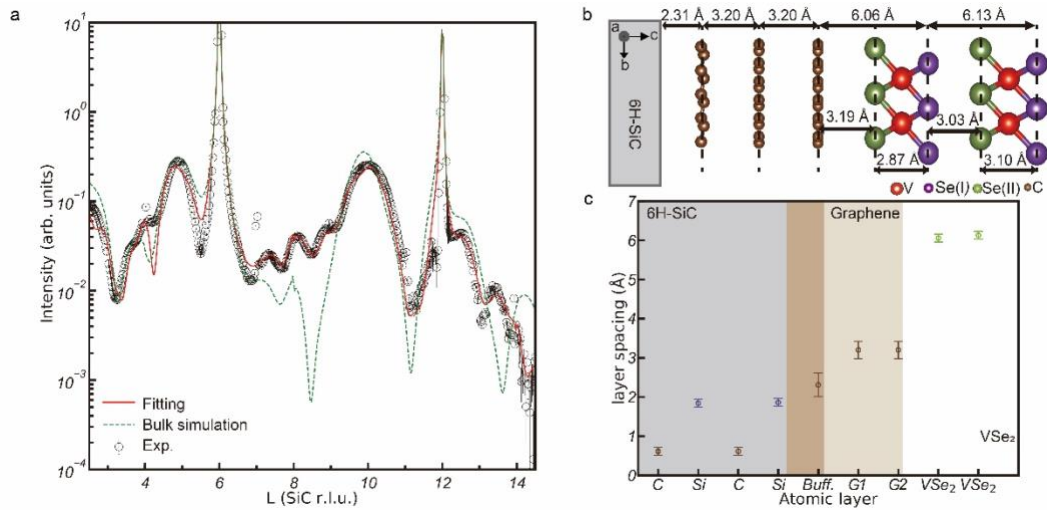
- <https://doi.org/10.1103/PhysRevB.102.115149>.
- [20] I.K. Robinson, D.J. Tweet, Surface X-ray diffraction, *Rep. Prog. Phys.* 55 (1992) 599–651. <https://doi.org/10.1088/0034-4885/55/5/002>.
- [21] E. Vlieg, *ROD*: a program for surface X-ray crystallography, *J. Appl. Crystallogr.* 33 (2000) 401–405. <https://doi.org/10.1107/S0021889899013655>.
- [22] E. Vlieg, S.J. Gurman, C. Norris, X-RAY DIFFRACTION FROM ROUGH, RELAXED AND RECONSTRUCTED SURFACES, (n.d.) 21.
- [23] A.S. Disa, F.J. Walker, C.H. Ahn, High-Resolution Crystal Truncation Rod Scattering: Application to Ultrathin Layers and Buried Interfaces, *Adv. Mater. Interfaces.* 7 (2020) 1901772. <https://doi.org/10.1002/admi.201901772>.
- [24] C.M. Schlepütz, R. Herger, P.R. Willmott, B.D. Patterson, O. Bunk, Ch. Brönnimann, B. Henrich, G. Hülsen, E.F. Eikenberry, Improved data acquisition in grazing-incidence X-ray scattering experiments using a pixel detector, *Acta Crystallogr. A.* 61 (2005) 418–425. <https://doi.org/10.1107/S0108767305014790>.
- [25] D. Waasmaier, A. Kirfel, New analytical scattering-factor functions for free atoms and ions, *Acta Crystallogr. A.* 51 (1995) 416–431. <https://doi.org/10.1107/S0108767394013292>.
- [26] I.J. Pickering, M. Sansone, J. Marsch, G.N. George, Diffraction anomalous fine structure: a new technique for probing local atomic environment, *J. Am. Chem. Soc.* 115 (1993) 6302–6311. <https://doi.org/10.1021/ja00067a052>.
- [27] B.L. Henke, E.M. Gullikson, J.C. Davis, X-Ray Interactions: Photoabsorption, Scattering, Transmission, and Reflection at $E = 50\text{--}30,000$ eV, $Z = 1\text{--}92$, *At. Data Nucl. Data Tables.* 54 (1993) 181–342. <https://doi.org/10.1006/adnd.1993.1013>.
- [28] Y. Yamashita, J. Nara, E.D. Indari, T. Yamasaki, T. Ohno, R. Hasunuma, Experimental and theoretical studies on atomic structures of the interface states at $\text{SiO}_2/\text{4H-SiC}(0001)$ interface, *J. Appl. Phys.* 131 (2022) 215303. <https://doi.org/10.1063/5.0093267>.
- [29] S. Pal, K. Debnath, S.N. Gupta, L. Harnagea, D.V.S. Muthu, U.V. Waghmare, A.K. Sood, Pressure-induced 1 T to 3 R structural phase transition in metallic VSe 2: X-ray diffraction and first-principles theory, *Phys. Rev. B.* 104 (2021) 014108. <https://doi.org/10.1103/PhysRevB.104.014108>.
- [30] D. Dale, A. Fleet, Y. Suzuki, J.D. Brock, X-ray scattering from real surfaces: Discrete and continuous components of roughness, *Phys. Rev. B.* 74 (2006) 085419. <https://doi.org/10.1103/PhysRevB.74.085419>.
- [31] J. Harada, Evaluation of the roughness of a crystal surface by X-ray scattering. I. Theoretical considerations, *Acta Crystallogr. A.* 48 (1992) 764–771. <https://doi.org/10.1107/S0108767392003246>.
- [32] J.D. Emery, B. Detlefs, H.J. Karmel, L.O. Nyakiti, D.K. Gaskill, M.C. Hersam, J. Zegenhagen, M.J. Bedzyk, Chemically Resolved Interface Structure of Epitaxial Graphene on $\text{SiC}(0001)$, *Phys. Rev. Lett.* (2013) 5.
- [33] A.J. Van Bommel, J.E. Crombeen, A. Van Tooren, LEED and Auger electron observations of the $\text{SiC}(0001)$ surface, *Surf. Sci.* 48 (1975) 463–472. [https://doi.org/10.1016/0039-6028\(75\)90419-7](https://doi.org/10.1016/0039-6028(75)90419-7).



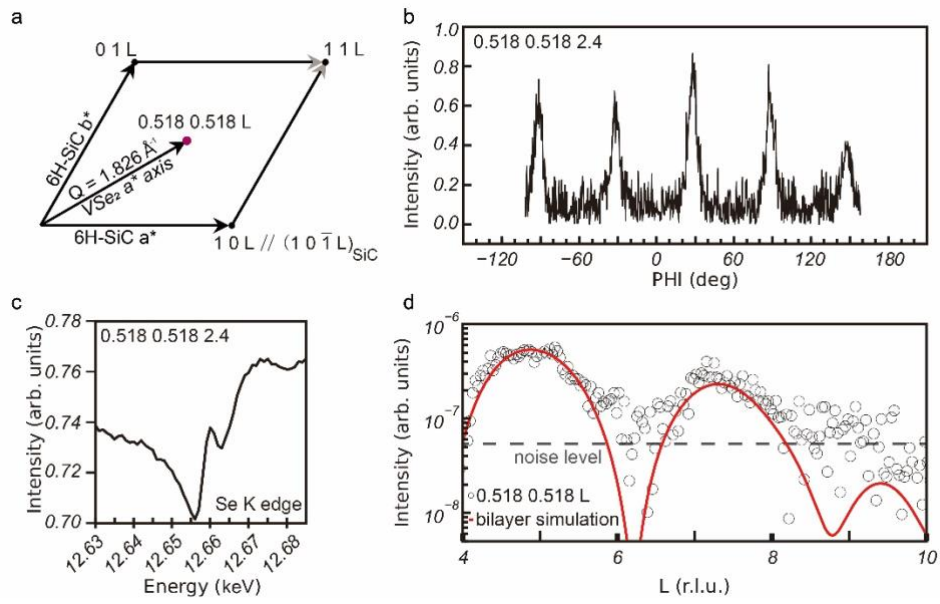
R. Kim *et al.*, Fig. 1.



R. Kim *et al.*, Fig. 2.



R. Kim *et al.*, Fig. 3.



R. Kim *et al.*, Fig. 4.